Low-Earth Orbit User Segment in the Ku and Ka-Band

Antennas and RF Front-End Technologies for the Ku and Ka Band LEO User Segment

Giandomenico Amendola, *Senior Member , IEEE* Daniele Cavallo, *Senior Member, IEEE,* Tobias Chaloun, *Member, IEEE,* Nicolas Defrance, *Member, IEEE,* Nelson J. G. Fonseca, *Senior Member, IEEE,* George Goussetis, *Senior Member, IEEE,* Marc Margalef-Rovira, *Member, IEEE,* Enrica Martini, *Senior Member, IEEE,* Oscar Quevedo-Teruel, *Senior Member, IEEE* Václav Valenta, *Member, IEEE,* Mauro Ettorre, *Senior Member, IEEE.*

I. INTRODUCTION

Low earth orbit (LEO) constellations are revolutionizing the world of satellite communications providing new opportunities to manufacturers and operators and enabling innovative and attractive services to users. The main advantages of low orbit satellite systems are:

- a more extended coverage of the surface of the Earth that permits the availability of Satcom links in areas not served by Geostationary Earth Orbit (GEO) systems;
- a reduced latency that proves to be fundamental for real-time and mission-critical applications;
- a reduced size of the user terminals due to the reduced path loss of low-orbit of satellites.

However, the benefits given by LEO satellites come with technical challenges. LEO satellites travel at high speed and can ensure the coverage of the targeted areas of the Earth's surface only for a limited time, placing stringent requirements on the antenna for both the space and ground segment. In particular, the antennas should be agile and able to steer their main beam over a large field of view. It is worth mentioning that the field-of-view of the antenna is related to the number of satellites of the constellations. A trade-off is therefore required to achieve a reasonable number of satellites and a feasible field of view for robust communications. Furthermore, LEO systems require handover between satellites to guarantee an uninterrupted link at the cost of a more complex system. The handover is achieved by radiating several beams or buffering the information in the antenna terminal.

In other terms, LEO links alleviate some of the drawbacks of the GEO systems but give new technological challenges in the design of antenna systems and Radio-Frequency (RF) front ends. The present paper attempts to provide a broad overview of the available RF technologies that allow the designers to tackle these challenges and help build the future LEO user segment.

The paper develops into six sections. Section II presents a brief account of the current LEO systems at the Ku/Ka-band by overviewing present and future constellations and providing information relevant to the development of the user segments. Section III defines very general requirements used as guidelines in the paper. Also, in this section, we identify the technologies presented in the following parts of the review. In a nutshell, the paper follows the structure of an RF front-end, starting from the antenna to go down towards the other components. For brevity, we have reduced the scope of this review to antennas, beamforming technologies, low noise amplifiers (LNAs), and power amplifiers (PAs). Notice that there are fields of research that are equally important and not included in the present work. As an example, the area of packaging and integration, which is of utmost importance to provide highly integrated solutions and of analog phase shifters will not be treated in this article. In section IV, we will review the most recent antenna solutions suited to LEO communications. We will present the antennas according to the scanning approach: mechanical or fully electronic. In section V, we discuss state-of-the-art beamforming technologies. We include analog passive beamformers and silicon active beamformers, as they are becoming a fundamental building block of electronically steerable antennas. As a final contribution, we account for recent developments in digital beamforming (DBF). While

The paper has been submitted for revision the 15/05/2022.
Giandomenico Amendola (g.amendola@dimes.unical.it) is with the Dipartimento di Ingegneria Informatica, Modellistica, Elettronica e Sistemistica, Università della Calabria, 87036 Rende (CS), Italy.
Mauro Ettorre (mauro.ettorre@univ-rennes1.fr) is with Univ Rennes, CNRS, IETR (Institut d'Electronique et des Technologies du Numérique), UMR 6164, 35000, Rennes, France.
Marc Margalef-Rovira and Nicolas Defrance are with Univ Lille, CNRS, Centrale Lille, Univ. Polytechnique Hauts-de-France, UMR 8520–IEMN-Institut d'Électronique de Microélectronique et de Nanotechnologie, F-59000 Lille, France.
Enrica Martini is with the Department of Information Engineering and Mathematics, University of Siena, 53100 Siena, Italy.
Oscar Quevedo-Teruel is with the Division of Electromagnetic Engineering, KTH Royal Institute of Technology, 11428 Stockholm, Sweden.
Nelson J. G. Fonseca is with the Antenna and Sub-Millimetre Waves Section, European Space Agency, 2200 AG Noordwijk, The Netherlands.
Daniele Cavallo is with the Microelectronics Department of the Electrical Engineering, Mathematics and Computer Science Faculty, Delft University of Technology, 2628 CD Delft, The Netherlands.
George Goussetis is with the School of Engineering and Physical Sciences, Institute of Sensors Signals and Systems, Heriot-Watt University, Edinburgh EH14 4AS, U.K.
Tobias Chaloun is with the Institute of Microwave Engineering, Ulm University, 89081 Ulm, Germany.
Vaclav Valenta is with ESA ESTEC, 2201 AZ, Noordwijk, The Netherlands.

TABLE I
MAIN PARAMETERS OF THE TELESAT, ONEWEB, STARLINK, KUIPER CONSTELLATIONS [1], [2].

	Telesat	OneWeb	Starlink	Kuiper
# of Satellites first phase-full constellation	298-1671	716-6372	1584-4408	578-3236
Altitude	1015 km-1325 km	1200 km	550 km-570 km	590 km-630 km
User link frequencies	Up: 27.5-30.0 GHz Down: 17.8-20.1 GHz	Up:12.75-14.5 GHz Down: 10.7-12.7 GHz	Up:14.0-14.5 GHz Down:10.7-12.7 GHz	Up:28.35-30 GHz Down:17.7-20.1 GHz

Downlink				
	Telesat	OneWeb	Starlink	Kuiper
# of User Beams	≥ 16	16	≥ 16	≥ 16
Channel BW	< 400 MHz	250 MHz	250 MHz	100 MHz
Max Antenna Gain	38 dB	NA	37.1 dB	39 dB
Max EIRP	39 dBW	34.6 dBW	32.71 dBW	43.1 dBW

Uplink				
	Telesat	OneWeb	Starlink	Kuiper
Channel BW	< 400 MHz	125 MHz	125 MHz	50 MHz
Max Antenna Gain	37.1 dB	NA	37.1 dB	39 dB
Max G/T	13.2 dB/K	-1 dB/K	9.8 dB/K	-

*Estimated considering altitude and maximum gain

DBF is not identifiable with one single device, it is one of the most promising technologies related to phased arrays and multi-beam antennas for future LEO Space and Earth segments. Finally, section VI reports the most relevant performance of LNAs and PAs.

II. KU AND KA LEO SYSTEMS

Despite the large investments dedicated to the development of LEO constellations, technical information on the communication technology adopted on board of satellites is rather scarce. In this section we summarize data available in the open literature to constitute a framework into which all the information reported in the next paragraphs can be placed. We consider constellations that are already in operation or in advanced development stages, i.e. Starlink, OneWeb, Telesat, and Kuiper [1]-[3]. The main constellations parameters are reported in Table I. The four constellations will be placed at low orbits with altitudes that may change according to the orbital planes on which satellites are allocated. Both user and feeder links operate in Ku and/or Ka frequency bands allocated to Satcom communications.

Table I reports information that can be used in a simplified link budget estimation.

The data reported in Table I indicate that the on-board resources provided by the constellations are abundant and, thanks to the multi-spot approach and the reduced altitude of the orbits, in most cases the design of compact and effective user terminals is possible.

III. CHARACTERISTICS OF LEO TERMINALS

The specifications of Satcom terminals vary greatly depending on the application and the data rate. The following section describes some of the characteristics of terminals with bit rates >20 Mbps, which are typical of broadband internet access services. Table II shows indicative Ku-band link budgets for the downlink and the uplink that consider a download data rate of 100 Mbps and upload rate of 20 Mbps. Satellite parameters are the ones of the Starlink constellation reported in [1], [2] which used the Federal Communications Commission (FCC) filings as sources. The diameter of the antenna is 0.7 m with aperture efficiency set to 30% to include the case of planar, phased array antennas. The receive (RX) RF front-end has a 1dB interconnection loss and a 3dB Noise Figure (NF). The

TABLE II
DOWNLINK AND UPLINK BUDGETS FOR A STARLINK BASED TERMINAL

Downlink		Uplink	
Data Rate	100 Mbps	Data Rate	20 Mbps
Frequency	11.5 GHz	Frequency	14 GHz
Satellite EIRP	32.71 dBW	Satellite G/T	9.8 dB/K
MODCOD	16-APSK(3/4)	MODCOD	16-APSK(3/4)
Roll off	0.2	Roll off	0.2
Elevation	40°	Elevation	40°
Path loss	168.47 dB	Path loss	170.18 dB
Atm.+ rain loss	1.89 dB	Atm.+rain loss	2.97 dB
RX Ant. Gain	33.3 dB	TX Ant. Gain	28.19 dB
RX Ant.Temp.	71.73 K	TX Ant.Temp.	-
Rx Ant. G/T	6.19 dB	TX Pin 1dB	5 W
C/ASI	25 dB	C/ASI	25 dB
C/XPI	22 dB	C/XPI	22 dB
C/IM	25 dB	C/IM	25 dB
Eb/(N0+I0)	11.51 dB	Eb/(N0+I0)	11.87 dB
Eb/N0	5.5 dB	Eb/N0	5.5 dB
Link Margin 99.9% av.	6.01 dB	Link Margin 99.9% av.	6.37 dB

downlink budget reported in Table II shows that the link margin at 99.9% availability is more than 6 dB. Note that even considering a receiver with 6dB NF and including scanning loss of 3 dB, the calculated link margin is greater than 2 dB.

The uplink budget considers a circular aperture with a diameter of 0.35 m and 5 W RF input power. This configuration roughly corresponds to a circular array of about 898 elements spaced at half a wavelength, fed with one amplifier per element with 7.5 dBm output power at a 1dB compression point. The

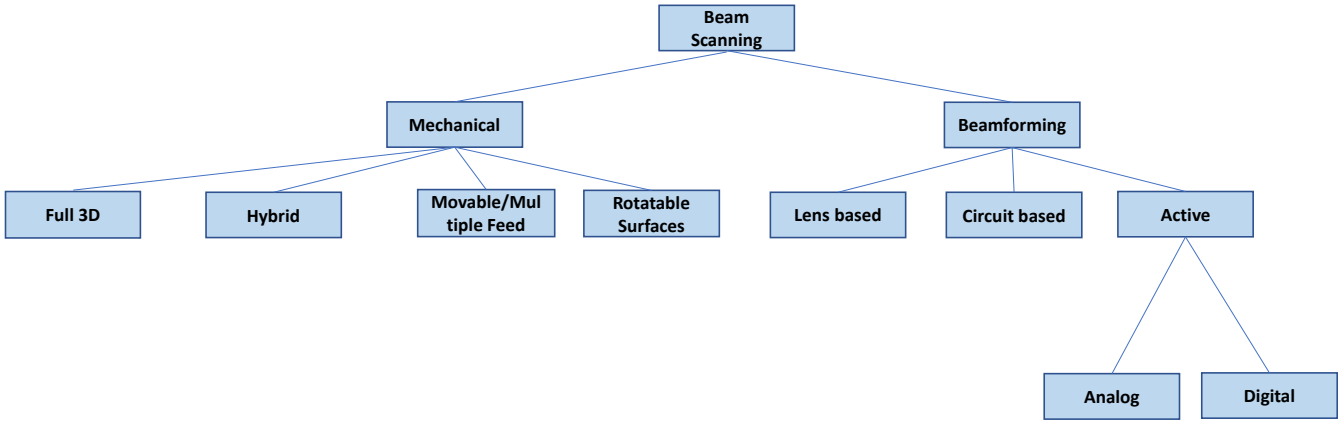

Fig. 1 Classification of Antennas and Beamforming techniques.

antenna aperture efficiency is 25%, lower than the one used in the RX case to account for the higher frequency of the TX band. Table II shows that the link margin is more than 6.4 dB and leaves room for 3 dB scan loss.

The evaluations presented above confirm that link budgets may be closed considering components with performances that are compatible with the state-of-the-art. However, considerable R&D efforts are still needed to design compact and flexible terminals. Difficulties mainly come from the requirement of scanning at low elevation angles and radiating two simultaneous beams and dramatically increase if one has to integrate TX and RX operations into a single aperture.

The architecture of the RF Front-end of an Earth terminal may change according to the antenna and the beamforming techniques that may combine to adapt to diverse requirements. Even if any attempt at a classification gives a partial view of all possible combinations, we refer to the grouping shown in Fig. 1. As LEO terminals must continuously scan the beam towards the moving satellites, the classification is according to the beam scanning techniques. In the subsequent sections, Fig. *1* is used as a reference reviewing antennas, beamforming, and semiconductor technologies for LEO terminals.

IV. Antennas

As LEO systems require terminals able to follow the satellites along their orbits, we classify antennas according to their scanning mechanism considering two very broad categories: mechanically scanned antennas and electronically scanned antennas. These two approaches present different degrees of maturity, performance, and costs. In the following, the two categories will be presented briefly explaining the principle of operation and describing their performances.

A. Mechanical Scanning

Mechanically scanned antennas offer an extended angular coverage with excellent performances in terms of polarization purity, band of operation, and G/T figure. Fig.1 proposes a classification of the available technologies that group mechanically scanned antennas into four broad classes: based on gimbals, allowing full three dimensional (3D) pointing , hybrid systems, moving feeds, and rotatable surfaces. The same classification is followed in the subsequent sections to present the characteristics of the antenna systems. Note that this classification is inevitably stretched, and while it covers most of the systems in use, it does not encompass all possible configurations. As an example, the class of hybrid systems covering more than one of the highlighted groups.

A.1 Full 3D pointing systems

Full 3D pointing requires complex mechanical gimbals. Many of these solutions rely on conservative concepts such as reflector antennas [5], [6]. Such antennas are generally bulky and heavy and may require a gimbal with at least two servomotors to control the pointing direction of the radiated beam and its polarization. Over the years, the profile of mechanically steered antennas was reduced to ease their integration in moving platforms such as airplanes. Solutions based on waveguide-based arrays [7] have been adopted because they have a lower profile and better efficiency than reflector antennas. However, they require complex pointing mechanisms that couple the azimuthal rotation with movement in elevation.

A.2 Hybrid systems

The complexity of the 3D pointing systems is reduced considering hybrid systems in which only the azimuthal rotation is achieved mechanically. Pointing in elevation is obtained by scanning the beam using conventional phase shifters, quasi-optical beamformers, or, in the case of lens antennas, adopting multi-feed systems or a moving feed. This last two cases are described in the next sections.

TABLE III
COMPARISON OF REPORTED KU- AND KA- BAND TX AND RX MECHANICAL AND HYBRID SOLUTIONS

Tx	Frequency band (GHz)	Technology	Polarization	Scan range		EIRP dBW	Gain (dBi)	Maximum scan loss (dB)	Aperture (cm) Thickness(cm)
				Azimuth	Elev.				
[27]	13.75-14.5 (Ku)	Rotatable VICTS	Tracking linear	360°	7.5°-90°	57.5 (PSat)	38*	4.5	75 (diameter)* 10.7
[12]	14-14.5 (Ku)	Hybrid phased array	Tracking linear	360°	15°-75° (16 beams)	-	36	4	64×19.2 22.5
Error! Reference source not found.	27.5-31 (Ka)	VICTS	Switchable circular	360°	7.5°-90°	55.5	38*	4.5	43.2(diameter) 9.1
[36]	30 (Ka)	Translating lenses	Circular	360°	50°-90°	-	27	3.3	11.9×11.9 12

Rx	Frequency band (GHz)	Technology	Polarization	Scan range		G/T dB/°K	Peak gain (dBi)	Maximum scan loss (dB)	Size(cm) Thickness(cm)
				Azimuth	Elev.				
[27]	10.7-12.75 (Ku)	Rotatable VICTS	Tracking linear	360°	7.5°-90°	18.5(peak)	39*	4.5	75 (diameter)* 10.7
[12]	12.25-12.75 (Ku)	Hybrid phased array	Tracking linear	360°	15°-75°	-	35	4	64×19.2 22.5
[13]	11.57-11.85 (Ku)	Hybrid phased array	circular	360°	15°-55°	10	31.5	<3	80(diameter) 13.5
[30]	11 (Ku)	Rotatable lenses	Single linear	360°	39°-90°	-	19.4	3	16.35×16.35 3.5
[32]	12.5 (Ku)	Rotatable lenses	Dual linear	360°	50°-90°	-	17.8	3	12.38×12.38 2.8

Different designs have been proposed in recent years for the Ku band in which a planar array is integrated with phase shifters to scan the beam in one direction, [11], [12]. In [13], the elevation beam steering is obtained through a switched beam architecture realized in microstrip technology in the form of a Rotman lens. Employing RF switches instead of phase shifters implies lower losses, higher simplicity, and lower cost. Planar quasi-optical beam formers like the Rotman lens have also the advantage to generate simultaneous independent beams, which can be used to realize a make-before-break handover between different satellites. Furthermore, their design generally relies on non-resonant true-time delay structures and is therefore intrinsically broadband. In particular, this implies that Tx and Rx functions can be combined into the same aperture possibly covering multiple bands. Lens-based concepts in parallel plate waveguide (PPW) technology have been introduced in Ka-band to preserve the wideband operation of reflector-based solutions and, at the same time, provide a wide coverage (±50° in elevation) [8].

A.3 Movable feeds and Multi-feeds systems

Another class of mechanically scanned antennas suited for Satcom communications are the volumetric lenses using movable feeds or multi-feed systems. They are seen as quasi-optical beamformers that may achieve a wide scan range with reduced antenna dimensions compared to reflectors. Volumetric lenses can be classified into two main categories:

-homogeneous lenses [14], whose scan range is limited by aberrations;

-graded-index lenses, which can be aberration-free.

Classical designs of graded-index lenses allowing beam scanning, like the Luneburg lens and the half Maxwell fish-eye lens [15], do not meet the low-profile requirement and may not be suitable for Satcom applications like Satcom-on-the-move. It is worth noting that arrays of smaller lenses can offer better efficiency than a single lens of a similar aperture, with a lower profile [16].

In recent years, the application of transformation optics concepts [17] was proposed to reduce the profile of the Luneburg lens. Scanning is obtained simply by displacing the

feed, at the price of an increased scanning loss and a reduction of the scanning range [18], [19].

A two-dimensional version of the Luneburg lens can provide full azimuthal coverage with a low-profile arrangement, and it can be used as a beamforming network for a radiating aperture. Practical realizations are normally done in parallel plate waveguides. Different solutions have been proposed to realize the required effective refractive index variation. This can be achieved by machining a distribution of metal posts between parallel-plate waveguide plates [20], photolithographically etching holes into one side of a standard PCB ground plane [21] and loading the parallel plates with electrically small patches printed on a grounded dielectric slab [22] [22]. A similar metasurface-based solution has been used in [23], [23] to implement a half Maxwell fish-eye lens. All-metal lenses realized by a fakir bed of nails or periodic holes in a thick metallic plate have also been presented [24], [25]. An alternative fully metallic solution is obtained in [26] relying on a geodesic principle. This solution has the advantage of an increased bandwidth compared to the ones based on dispersive modulated metasurfaces. Furthermore, it is scalable to high frequencies due to the lack of small geometric details. However, it has a larger thickness when compared with its fully planar counterparts. Note that in all the two-dimensional lenses reported until now, scanning is achieved by displacing the feed or implementing a multi-feed system.

A.4 Rotatable surfaces systems

Low-profile antennas with full 2D scanning may be implemented using rotatable surfaces. The most performing antenna terminals in Ku- and Ka-band in this category are designed by ThinKom. ThinKom's antennas are based on VICTS (Variable Inclination Continuous Transverse Stub) technology, an array of stubs rotating around a single axis for a wide field of view and operating band [27], [28]. The terminal provides interoperability between different constellations with a large field-of-view (7.5°-90° in elevation) and very appealing G/T performances (>12 dB/K at 20°elevation). It is worth mentioning that mechanical solutions do not generally have multiple beam radiation. Information is then buffered to switch between satellites requiring rapid control of the radiated beam.

2D scanning is also achieved with rotatable graded index lenses placed in front of a radiating aperture. The principle of operation is similar to the so-called Risley prisms. In this solution, a fixed primary radiator with a broadside pencil beam illuminates two parallel planar lenses providing a linear phase shift. The two lenses can be rotated either synchronously or independently around the axis of the primary radiator to steer the beam in the upper hemisphere. The resulting architecture is significantly simpler and less bulky than the typical Az/El (Azimuth/Elevation) positioner used for reflector antennas, and its profile remains unchanged while the beam is scanned. The screens needed are passive and they do not contain reconfigurable elements. The feasibility of the scanning mechanism based on rotatable metalenses was first demonstrated in [29] using a horn as the primary feed. More recent works have achieved higher aperture efficiency and smaller thickness using a low-profile primary radiator [30]-[34]. The main challenge in the design of this kind of antenna for Satcom applications is the control of grating lobes during scanning, which is strictly related to the design of the metalenses.

A similar solution is based on translating lenses: in this case, steering in elevation is achieved by lateral translation of a thin flat lens placed a few wavelengths above a feed antenna, whereas azimuth steering is achieved by rotation of the lens or both the lens and the feed horn [35]. Dual-band operation and beam steering range up to 50° have been demonstrated [36].

Table III summarizes the recent developments for antennas based on mechanical and hybrid scanning for Ku and Ka-bands.

B. Electronic Scanning

Electronic beam steering antennas are the optimal solution for satellite tracking, especially when reliable and agile operation is desired. Electronic scanning is particularly advantageous for Satcom on-the-move systems (e.g., on aircrafts), which require flat antennas that can rapidly repoint to the satellite to compensate for the platform motion. Other than this, fully electronic active arrays can provide various reconfigurability characteristics, radiation pattern shaping, wide scanning capability, multiple-beam generation, and power sharing among beams through distributed amplification.

Despite the extended capabilities offered by phased arrays, the high cost and complexity of such antennas have for long time limited their widespread use in commercial systems. For this reason, several approaches have been proposed to realize cost-effective electronic scanning antennas, including tunable reflectarrays and transmitarrays [36]-[41] and liquid crystal based antennas [42], [43]. However, the typical components used for tuning the elements, such as PIN and varactor diodes, Micro Electro-Mechanical Systems (MEMS), and liquid crystals, are associated with increased dissipation losses.

Recent developments of electronic chipsets with lower cost and higher power (see Sec. V) have significantly contributed to a renewed interest in active array antennas.

More specifically, the cost of fully active phased arrays has recently dropped thanks to the advance of silicon multi-channel chips to be used for transmit/receive (T/R) modules [44] paving the way to the realization of Satcom phased arrays that are now commercially available.

Recent literature reports the performance of numerous Ku- and Ka-band phased arrays. A comparison between the measured EIRP and G/T for transmitting (Tx) and receive (Rx) cases, respectively, of different prototypes is reported in Table IV. Regarding the scanning capability, the need for terminal antennas able to scan to larger angles is emerging to guarantee agile connections to different satellites. However, conventional planar phased array antennas exhibit limitations when steering a pencil beam in a large field of view. The first is the deterioration of the antenna active reflection coefficient when scanning at low elevation. The issue is solved with an extensive optimization process of the radiating elements and the array lattice, and with the help of matching layers. However, even

TABLE IV
COMPARISON OF REPORTED KU- AND KA- BAND TX AND RX PHASED ARRAYS

Tx	Frequency band (GHz)	Antenna elements	Number elements	Polarization	Scan range	Max EIRP (dBW) @P1dB	Scan loss at max. scan angle (dB)	Aperture size (cm^2)
[46]	12-14.5 (Ku)	Stacked patches	4×4	dual	$\pm 40^\circ$	7.5 @12.5 GHz	≈ 3	10×7
[47]	13-14.6 (Ku)	Stacked patches	16×16	dual	$\pm 60^\circ$	34 @14 GHz	≈ 5	17×17
[48]	14-14.5 (Ku)	Stacked patches	32×32	dual	$\pm 75^\circ$	44 @14.25 GHz	≈ 7	28.9×33.2
[50]	29.5-30 (Ka)	Stacked patches	32×32	dual	$\pm 60^\circ$	44 @29.7 GHz	≈ 4.5	16×16
[51]	27.5-31 (Ka)	Patches	16×16	single	$\pm 70^\circ$	34.5 @30 GHz	≈ 4	≈ 8×8
[52]	26.5-29.5 (Ka)	Patches	8×8	dual	$\pm 50^\circ$	24 @28 GHz	≈ 5	7×7

Rx	Frequency band (GHz)	Antenna elements	Number elements	Polarization	Scan range	G/T (dB/K)	Scan loss at max. scan angle (dB)	Aperture size (cm^2)
[51]	27.5-31 (Ka)	Patches	16×16	single	$\pm 70^\circ$	-1	≈ 4	≈ 8×8
[54]	11.7-12.2 (Ku)	Patches	94	dual	$\pm 60^\circ$	0.9	≈ 4.1	24×25
[55]	10.6-12.5 (Ku)	Patches	16×16	dual	$\pm 70^\circ$	5.4	≈ 5 to 8	22.2×19.7
[56]	10.9-12.6 (Ku)	Stacked patches	156	dual	$\pm 70^\circ$	0.3	≈ 7.4	$\pi(11)^2$
[58]	10.7-12.7 (Ku)	Patches	32×32	dual	$\pm 70^\circ$	10.5	≈ 8	39×34

when a good matching is achieved for wide scan angles, the diminished aperture projection (proportional to $\cos\theta$, where θ is the scan angle) translates into a reduced antenna gain. For this reason, a tradeoff is in order between the use of conformal or multi-panel arrays [59], curved radomes that increase the scan range [60]-[63], and combination of electronic scan with a small mechanical tilt [64].

Another known limitation of current Satcom phased arrays is the narrow bandwidth that forces to use multiple antennas to cover different frequency bands. In applications that require terminal mounted on mobile platforms, the space available is often limited and the presence of two antennas is a major drawback. In this regard, it may be beneficial to use a wideband array covering simultaneously multiple bands [64]-[66]. This solution may reduce the volume and costs of the system, including fuel costs created by the weight and drag from the antennas. Note that, in wideband arrays, the isolation between different bands and TX and RX channels is a further difficulty that makes the design cumbersome.

VII. BEAMFORMERS

Beamforming may be achieved in many ways with performance that may change considerably if complexity, flexibility, and costs are considered. In this paper we will review three main classes of beamforming:

- analog, circuit based, passive beamforming with a limited number of orthogonal beams;
- analog active beamforming, based on highly integrated silicon beamformers, implementing phased array functionalities.
- digital beamforming.

A. Analog, Circuit-Based, Passive Beamforming

Analog beamforming solutions are typically well adapted for array antennas with a moderate size and a limited number of beams, typically a single beam or maybe two for user segment applications requiring a make-before-break handover [67]. These are of interest for LEO constellation systems with medium gain requirements, such as internet of things (IoT) terminals, where a conventional analog beamforming network may be an acceptable solution in terms of complexity and performance. Over recent years, there has been a regain of interest for analog solutions based on orthogonal beamforming networks [68]. Most works are based on the well-known Butler matrix [69]-[72], and some also considered the less known Nolen matrix [73]-[76]. A general form of parallel orthogonal beamforming network for single-layer implementation has also been proposed recently [77], as beamforming theory is still an active field of research. A comparison of these different beamforming matrices is provided in Table V. Most papers focus on practical implementations, with particular interest on millimeter-wave designs and more specifically 5G terrestrial communications enabling interesting synergies with satellite communications in Ku and Ka-band. Solutions based on low-cost substrate integrated waveguide (SIW) technology [78] are particularly appealing for applications which require cheap mass-produced terminals, such as maritime transport asset tracking.

Orthogonal beamforming matrices have the advantage of producing multiple beams while avoiding recombination losses inherent to standard corporate networks [68]. These are generally used in a beam-switching configuration or in simultaneous multiple fixed beam operation, although some works have explored the capability they offer to combine beam switching and beam steering [79]-[81]. Because their complexity generally increases exponentially with the number

TABLE V
COMPARISON OF ANALOG BEAMFORMING MATRICES WITH M INPUT PORTS AND N OUTPUT PORTS

Matrix Type	Design Examples	Number of beams	Number of Couplers	Number of Phase shifters	Number of Crossovers	Frequency Response	Design Implementation
Butler matrix*	[70]-[72]	$M = 2^n$	nN/2	(n-1)N/2	(N-n-1)N/2	Broadband to Wideband	Preferably Dual-Layer
Serial Nolen matrix	[74]	$M \leq N$	M(2N-M-1)/2	M(2N-M-1)/2	0	Narrowband	Very Compact Single-Layer
Parallel Nolen Matrix	[75], [76]	M = N	N(N-1)/2	N(N-1)/2	0	Broadband	Single-Layer
Generalized Parallel Matrix	[77]	M = N	N(N-1)/2	N(N-1)/2	0	Broadband	Compact Single-Layer

*Assuming a standard form with 4-port couplers as building blocks, $N = 2^n$.

of beams, most designs reported are limited to 4×4 and 8×8 matrices, with some rare examples of 16×16 Butler matrices [82]-[84]. For larger arrays, a hybrid beamforming approach combining typically analog beamforming at sub-array or tile level and digital beamforming at array level is considered a promising approach to combine the benefits and mitigate the drawbacks of both technologies [85],. Compared to a fully digital implementation the hybrid beamforming antenna system also has N radiating elements, but only N/2 RF chains instead of N on the fully digital beamforming antenna system. The sub-arrays may be fixed or reconfigurable, possibly including amplitude and phase control in a fully reconfigurable design. The analog part may be further extended to have multiple inputs and multiple outputs, with one RF chain per input port. Using orthogonal beamforming matrices in the analog part enables a more efficient design at the expense of scanning range restrictions.

B. Analog Active Beamforming

Beamforming ICs interface the antenna elements and beam-splitting / combining networks. In TX, their role is to map input signals to multiple outputs with specific gain and phase coefficients that correspond to the specific position of the antenna element. In the RX direction the functional role is reversed and in addition an adequate low noise figure is needed to guarantee the required G/T since, in most of the active Satcom arrays the beamforming, IC is interfacing directly with the radiating elements without external LNA. Today, there is a range of commercial-of-the-shelf (COTS) beamforming ICs available on market, covering X, Ku, Ka and even Q/V bands. They come in various configurations, e.g., in multi-channel architectures where for instance four inputs are mapped to four outputs, i.e., containing 16 amplitude and phase control nodes [87]. Other configurations incorporate the signal combining and splitting functions [88] or even down-converting functions to enable beamforming at digital level [89]. Unlike 5G beamforming, Satcom active antennas have larger apertures and use larger communication bandwidth and hence beam-squint effects need to be considered. For this reason, the beamforming IC should cover the necessary delay to compensate for dispersion across the antenna aperture. Low DC power, often referred per single beamforming node, is also of very high importance as the beamforming ICs contribute significantly to overall power consumption of the active array. Low-power beamforming ICs available on market today consume less than 10 mW per beamforming node but they have a P1dB of less than 0 dBm. Consequently, an additional output amplification is used to reach the output power level required by Satcom links. The main contribution determining the power consumption is coming from the on-chip gain blocks that compensate splitting losses and losses of amplitude/phase/time delay control blocks. The losses of these elements are minimised thru an accurate choice of the beamforming architecture and of the integration technologies. As an example, losses of transmission lines can be reduced by design techniques such as thin-film microstrip (TFMS) that shield the line from lossy low-resistivity silicon substrates in SiGe BiCMOS implementation. As far as Silicon-on-Insulator (SOI) technologies are concerned, the inherent physical properties of the insulator, will offer higher isolation between channels and low-loss implementation of switching functions and high-Q inductors allowing superior performance. This is evident looking at the NF performance. SOI 22 nm and 45 nm nodes have recently demonstrated a NF below 1.5 dB, approaching the state-of-art levels obtained in GaAs [91].On the other hand, considering the P1dB required by Satcom application, SiGe BiCMOS with higher voltage breakdown levels will outperform RF-SOI amplifiers by several dB. Furthermore, SiGe performances are achieved without applying transistor stacking techniques and avoiding the risks associated with the time-dependent dielectric breakdown which is known to be one of the most important degradation mechanisms affecting the reliability of CMOS devices [90].

Availability of wafer level packaging solutions for a given technology is another important aspect to consider, to facilitate array assembly and allow for proper thermal management which is a particular challenge for SOI. Suitable wafer level packaging techniques advance rapidly together with semiconductor processes and for instance, the maturity of wafer level packaging such as Embedded Wafer Level Ball Grid Array (eWLB) has been proven also at mm-wave frequencies [92], [93].

C. Digital Beamforming

LEO constellations are foreseen to deliver high-throughput broadband and ubiquitous services with low latency. The envisioned scenario, however, will necessitate the user terminal to track multiple satellites simultaneously in terms of position

TABLE VI
INDICATIVE TRADE-OFF FOR THREE SELECTED PROCESSES ADOPTED IN MOST BEAMFORMING ICS: TWO RF-SOI TECHNOLOGY NODES AND SIGE BICMOS

Technology	NRE costs	Cost /Area for amplifier	Wafer process time	Integration density	Thermal management	Voltage breakdown	P1dB	PAE	NF
RF-SOI for mm-waves	baseline		~ 8-12 weeks	• • •	•	•	•	• •	• • •
RF-SOI for Ku&Ka bands	< ½ of baseline	baseline	~ 8-12 weeks	• •	•	• •	• •	• •	• • •
SiGe BiCMOS	~ 1/10 of baseline	2 x baseline	~ 10-15 weeks	•	• • •	• • •	• • •	• • •	• •

as well as polarization to provide truly uninterrupted operation. Although analog beamformers offer the unparalleled capability to realize single beam phased array antennas with low hardware complexity and power consumption, analog beam steering poses severe challenges when designing point-to-multipoint antenna systems. In particular for higher operating frequency in the micro- and millimeter-wave regime, spatial multiplexing systems based on analog beamformers commonly suffer from inherently space constraints because the amount of analog circuitry is inevitable linked with the number of independent beams. In contrast, multi-beam antenna systems using digital beamforming (DBF) do not show these limitations as they perform the namesake function solely in the digital back-end [94]. This leads to a simplified RF chain per antenna element basically comprising an amplification and frequency conversion stage for transmit and receive, respectively. DBF processing on element-level accompanies with the highest degree of flexibility in synthesizing multiple beams simultaneously because the transmit and receive signals at each antenna element can be arbitrarily manipulated, duplicated, and combined in the digital domain and hence avoiding signal-to-noise ratio (SNR) degradation. Furthermore, unlike their analog counterparts, fully digital beamformer processors can seamlessly apply frequency-dependent amplitude tapering and phase shifting enhanced by the possible compensation of hardware impairments through channel-level equalization, I/Q balancing, static local oscillator (LO) phase offsets at each antenna element [95].

Pushed by the ambitious data throughput goals of near-future LEO/MEO satellite communications, DBF-based antenna terminals are becoming an interesting design approach to cover large instantaneous bandwidths, while avoiding the use of analog true time delay elements [96]. Despite all these advantages, the implementation effort of the signal processing back-end strongly scales with the number of antenna elements as well as system bandwidth [97]. Ahead of their time, the first DBF antenna modules for mobile Satcom terminals at 30 GHz have been presented in [98], [99]. In these pioneering works, the digital baseband processing unit supports the control of up to 64 radiation elements within a signal bandwidth of a few tens of MHz. A situation radically different from 10 years ago, when the use of COTS components ruled the active antenna design, the custom development of application-specific integrated circuits (ASICs) for specific commercial sensor and communication applications have become very much mainstream now. An example for the current generation of DBF ASICs for the SatCom market segment is the SatixFy's Prime [100]. The true time delay DBF chip supports up to 32 antenna elements and can be connected with each other to span large antenna apertures. The individual signals at each antenna element are translated between the analog and digital domain by high-speed analog-to-digital converters (ADC) and digital-to-analog converters (DAC), respectively.

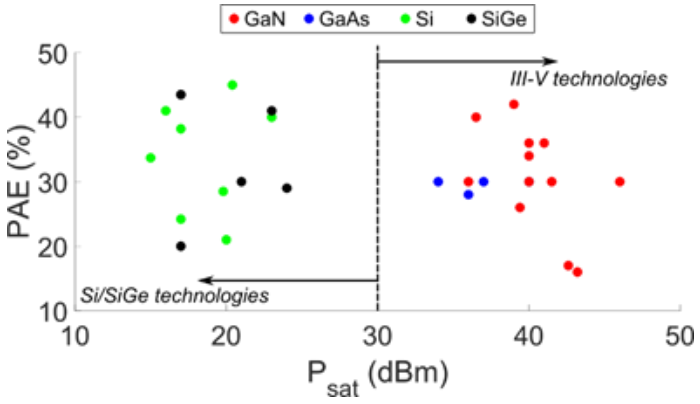

Fig. 2. P_{sat} versus PAE of current state-of-the-art GaAs [111],[112], GaN [111],[112], and Si [117]-[124] and SiGe PAs [125]-[129] in the Ku/Ka frequency bands.

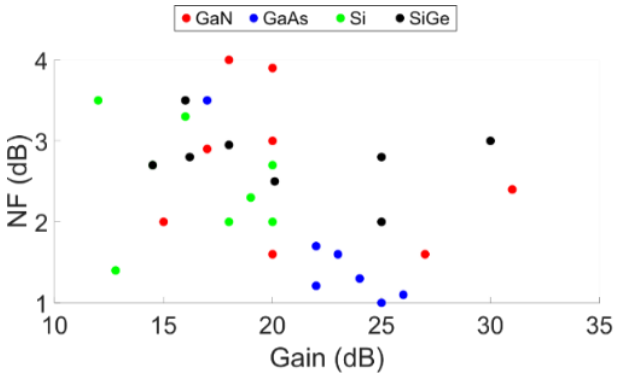

Fig. 3. Gain versus NF of current state-of-the-art GaAs [111],[112], GaN [111],[112], SiGe [131]-[138] and Si [130],[139]-[145] LNAs in the Ku/Ka frequency bands.

Apart from high-resolution digital phase shifters and digital delay circuits, the signal processing inside beamformer ASIC may also correct RF front-end imperfections enabling wideband signal transmission and reception across 1 GHz of bandwidth in single beam mode. The enormous advances in CMOS semiconductor technologies have also enabled the commercial realization of data converters for direct RF sampling up to the Ka-band [101]. The latest trends show that digital beamformer ASICs enhanced by direct sampling up to Ka band are going to be deployed in future satellite payloads and thus circumvents the need for frequency conversion stages [102]. Although this all-in-one digital beam forming technology is not yet competitive to be used on element level in mobile DBF antenna terminals, the availability of high-performance data converters have paved the path for new code-based beamforming architectures [103]. In [103], more specifically, a code division multiplexing technique has been proposed to aggregate the individual signals from the antenna elements at the analog RF front-end into a single ADC. Compared to conventional digital beamforming techniques, a remarkable reduction of the number of required ADCs has been demonstrated, which in return must feature a higher sampling rate and analog bandwidth.

VI. Semiconductor Technologies

The integration level offered by Monolithic Microwave Integrated Circuits (MMICs) is a key feature for LEO constellations. Integration process have advanced considerably making possible the design of complete Systems-on-Chip (SoCs) in the frequency band considered in this review (i.e., Ku/Ka-bands). In this scenario, four main semiconductor families appear as attractive candidates for the aimed frequency bands and performances: (i) GaAs, (ii) GaN, (iii) SiGe, and (iv) Si.

The two former technologies belong to the wide bandgap semiconductor family, which intrinsically leads to greater output powers, and reduced NF. On the other hand, Si- and SiGe-based technologies present reduced footprints, higher gains, and the possibility of integrating digital control circuitry in a single die together with the RF function.

Considering power and bandwidth, GaN really emerges as the winner when faced to the competing technologies. In fact, progress in GaN device technology is considered crucial to the viability of power amplification in space and other critical applications in the future. In the past decade, GaN MMICs and discrete GaN devices have significantly improved their efficiency, power density, reliability, and overall output power. In the frequency bands considered in this review, Ku and Ka bands, GaN-based devices, and circuits already demonstrated superior performance in all these figures of merit while simplifying MMIC architectures and minimizing overall product footprint. Nevertheless, GaN-based MMICs are undergoing further research and development efforts accompanied by considerable investments to improve efficiency, output power and advance manufacturing processes

and module packaging. Note that prepackaged devices or carriers are still being employed as the most convenient and cost-effective means of building high power SSPAs for lower frequencies, typically below 30 GHz.

As far as GaAs is considered, this technology offers the non-negligible advantage of a lower noise and to integrate with CMOS technologies. Also, GaAs allow for the design of complete core chips that integrate into T/R modules.

The second family, (iii) and (iv) in the list presented above, is Silicon based. SiGe offers Heterojunction Bi-Polar Transistors (HBTs) in addition to MOSFETs [104]. Even though MOSFETs integrated in a 130-nm process can comfortably address the Ku/Ka-bands with respectable performances, HBTs offer much better performances, usually at the price of a more expensive technology. Modern pure silicon technologies offer additional features such as Silicon-On-Insulator (SOI) substrates that have effectively pushed forward the performance of these technologies, especially in terms of NF [105], as it will reported later in the paper.

The choice between the technologies briefly described up to now is usually driven by four principal drivers: (i) power output, (ii) Noise Figure, (iii) footprint, and (iv) costs.

The first two drivers determine the performances of a satellite terminal and the quality of the link in terms of availability and data rate. For this reason, in the succeeding sections, the state of the art of power amplifiers and LNAs will be overviewed in greater detail. The footprint of the device directly affects the level of integration achievable. The area of the devices is a critical parameter affecting the realization of electronically scanned antennas and phased arrays. In fact, phased arrays require that the distance between radiating elements is less than half of a wavelength. The last driver, costs, is probably the most difficult to evaluate and it will be only marginally considered. In fact, technology selection involves a complex trade-off between variables that affects costs, such as the technology type and node, volume, expected circuit complexity (~ die area), production wafer size, or process availability (i.e., wafer fab process time). Costs are critical in terminals that adopt phased array antennas because of the number of components. In these cases, Si-based technologies are the ones that offer the best level of integration. Silicon technologies have one principal cost factor in NRE (non-recurring costs), mainly related to the mask set. In the case of RF-SOI technology, NRE costs are absorbed only under a large production volume. While for SiGe, NRE costs could be several times lower than those of advanced SOI nodes (e.g., 130 nm SiGe vs. advanced RF-SOI). It is evident that SiGe will make sense in Satcom communications, where lower volume and high-end RF performance (e.g., higher linearity, higher P1dB, lower NF) are required. Several foundries have recently improved this trade-off for SiGe BiCMOS by moving from 200 mm to 300 mm wafers enhancing production efficiency and making SiGe suitable even for a large market above Ku-band. The indicative trade-off for SiGe and RF-SOI technologies is presented in Tab. VI.

A. Power amplifiers

The design of RF power amplifiers focuses on increasing the output power and optimizing the DC to RF efficiency. Consequently, benchmarking a power amplifier's saturation power (P_{sat}) and its Power-Added-Efficiency (PAE) provides a straightforward way to determine its performance.

Fig. 2**Error! Reference source not found.** presents a scatter plot of the current state-of-the-art PAs, comparing their PAE versus P_{sat}. In applications involving high data rate communication using higher-level modulation methods, other factors such as linearity or Noise Power Ratio (NPR) intervene to determine an efficient and robust communication link. versus their PAE.

Fig. 2**Error! Reference source not found.** shows a clear separation between III-V technologies (i.e., GaAs and GaN) and Silicon technologies symbolically delimited by the 30 dBm barrier due to the difference in operating voltage between III-V and Si-based technologies. Power amplifiers of the III-V group require a voltage around 12-28 V, while Silicon amplifiers need a voltage between 1 and 4 V.

GaN appears as a superior candidate for the design of PAs compared to GaAs and is becoming the technology of choice across frequency and markets. GaN amplifiers present a P_{sat} in the 36-46 dBm range [106]-[112] while the GaAs counterparts are within the 34-40 dBm range [111]-[116]. In addition, GaN PAs also show superior PAE, which can surpass 40%, while GaAs PAs present PAEs of the order of 30%.

Initially, higher output power and smaller form factors were the focus of GaN product development. However, the resulting thermal constraints at the system level push R&D efforts to achieve a better balance with efficiency to help reduce dissipated power and ease the thermal load at the system level.

In Si-only technologies, output powers of around 23 dBm have been reached [117] in Doherty-based PAs. On the other hand, with single-ended architectures that do not rely on power-combining techniques, most Si-based technologies tend to offer P_{sat} levels in the 14-20 dBm level [118]-[124]. In their turn, at these frequencies, these technologies tend to report PAE levels in the 20-45% range [117]-[124]. Finally, concerning the linearity of silicon-based PAs, they tend to show Output 1-dB Compression Points (OCP1dB) of around 1 to 1.5 dB below P_{sat} [117]-[124].

On the other hand, SiGe technologies with their HBT transistors feature P_{sat} in the 17-23 dBm [125]-[129] associated with PAE levels of around 30-43%.

Note that, compared to III-V technologies, the differences of the performance of PAs in pure Silicon and SiGe technologies is not sufficient to determine the choice of a given technology in this band. A clearer difference appears when operating frequencies move to greater ranges, where the performance of SiGe-HBTs clearly overpasses those of silicon-based MOSFETs.

B. Low Noise Amplifiers

The LNA is employed in satellite applications front-end receivers to amplify the degraded RF signals captured by the antenna to the desired level. The LNA boosts the received signal power by adding minimal noise and distortion to mitigate the impact of noise added by the components of the RF receiver chain. Its effect is to improve the signal-to-noise ratio (SNR), which is essential for the quality of the radio link. Design requirements combine the minimum NF with the high gain and

pose severe challenges to the designer. The complexity of the design further increases if one considers the problems of impedance matching, low power consumption, linearity, and stability.

Fig. 3**Error! Reference source not found.** presents the NF versus gain of current state-of-the-art GaAs [111],[112], GaN [111],[112], SiGe [131]-[138], and Si [130],[139]-[145] LNAs in the Ka/Ku frequency bands. LNAs based on GaAs dominate the low-NF part of the plot, followed by GaN devices. Note that low-NF LNAs can also be built with Silicon-On-Insulator platforms [130]. High gain LNAs are achievable with SiGe and GaN processes as well. GaN LNAs ensure good RF performance under low dc power consumption, which is a fundamental requirement for space and ground segments [147]. The latter is often achieved by reducing the nominal bias point to operate GaN HEMTs in low-current density area.

Concerning Si- and SiGe-based technologies, SiGe is more suited for the design of high-gain LNAs while pure Si-based processes offer better NF thanks to the Silicon on Insulator technology. LNAs with 30-dB-gain LNAs realized with a 0.13-µm BiCMOS process have been reported [131].

SiGe LNAs present NF in the 2-3 dB range in the Ka/Ku bands with gains that span the 15-30 dB range [131]-[138]. Silicon-based LNAs present more modest gain levels in the 12-20 dB range but show NF close to those of GaAs (i.e., nearly 1 dB) up to 3.5 dB [130],[139]-[145].

LNA performance is not only limited by the intrinsic gain and NF of a given transistor in a technology. The NF is largely impacted by the matching network required to adapt the input/output impedance of the transistor to 50 Ω, typically. Hence, the quality factor of passive devices in a certain technology will greatly limit the performance of an LNA.

Moreover, other parameters should be considered. For instance, LNAs are known for being particularly sensitive to high-power RF inputs that can put them into breakdown mode. Among the considered technologies, GaN can withstand the greatest amounts of power without entering a breakdown regime, followed by GaAs and SiGe, in that order. Recently, it was reported of GaN LNAs' surviving input power levels over 30 dBm continuous wave (CW) and nearly 50 dBm in pulse conditions. Moreover, GaN LNAs' demonstrated high linearity with third-order output intermodulation points (OIP3s) around 40 dBm [147].

Electro-Static Discharges (ESD) can also present a threat for most LNAs. For this reason, ESD must be carefully studied. Note that extra circuitry must be added to protect the LNA against ESD events, which can degrade the performance of the circuit. Hence, choosing a technology that is more resilient against ESD events may not only ease the design of an LNA but also dictate the choice between two technologies. For instance, SiGe LNAs have appeared as more robust against this kind of event than GaAs LNAs [146].

V. Conclusion

The present review provides a general outline of the current technologies for satellite user terminals. Even though the technologies reported are common to GEO and LEO applications, the focus was on the last case. Starting from the antenna, the review covered the various components of a user terminal, including the antenna, beamforming network, and LNAs and Pas. Comparative tables were provided for the reader to get a quick overview of the available technologies.
The proposed material is suitable for researchers seeking an overview of the current state of the art in the field. It is the authors hope that the paper will prove useful to researchers and engineers working in the field.

.References

[1] I. del Portillo, B. G. Cameron, E. F. Crawley, “A technical comparison of three low earth orbit satellite constellation systems to provide global broadband,” Acta Astronautica, Volume 159, pp. 123-135, 2019.
[2] N. Pachler, I. del Portillo, E. F. Crawley and B. G. Cameron, “An updated comparison of four low earth orbit satellite constellation systems to provide global broadband," 2021 IEEE International Conference on Communications Workshops (ICC Workshops), pp. 1-7, 2021.
[3] Starlink Exhibit 1 Supplemental Information Regarding EarthStations(https://apps.fcc.gov/els/GetAtt.html?id=197812&x=.)
[4] SatMaster Pro MK10.4d, Arrow Technical Services UK.
[5] https://orbit-cs.com/wp-content/uploads/2021/08/Orbit-MPT-DS-v0.03.pdf
[6] https://www.viasat.com/content/dam/us-site/antenna-systems/documents/1229461_G-18L_KuKa_Datasheet_006_web.pdf
[7] https://www.viasat.com/content/dam/us-site/antenna-systems/documents/1229461_KuKarray2L_Datasheet_005_web.pdf
[8] T. Ströber, S. Tubau, E. Girard, H. Legay, G. Goussetis, and M. Ettorre, “Shaped parallel-plate lens for mechanical wide-angle beam steering,” IEEE Trans. Antennas Propag., vol. 69, no. 12, pp. 8158 - 8169, Dec. 2021.
[9] M. Smierzchalski, F. Foglia Manzillo, M. Del Mastro, N. Capet, B. Palacin, R. Sauleau, and M. Ettorre, “A novel dual-polarized continuous transverse stub antenna based on corrugated waveguides -part I: principle of operation and design,” IEEE Trans. Antennas Propag., vol. 69, no. 3, pp. 1302-1312, Mar. 2021.
[10] M. Smierzchalski, F. Foglia Manzillo, M. Del Mastro, N. Capet, B. Palacin, R. Sauleau, and M. Ettorre, “A novel dual-polarized continuous transverse stub antenna based on corrugated waveguides - part II: experimental demonstration,” IEEE Trans. Antennas Propag., vol. 69, no. 3, pp. 1558-2221, Mar. 2021.
[11] F. Tiezzi, S. Vaccaro, D. Llorens, C. Dominguez and M. Fajardo, “Ku-band hybrid phased array antennas for mobile satellite communication systems,” 2013 7th European Conference on Antennas and Propagation (EuCAP), 2013, pp. 1605-1608.
[12] G. Han, B. Du, W. Wu and B. Yang, “A Novel Hybrid Phased Array Antenna for Satellite Communication on-the-Move in Ku-band,” IEEE Trans. Antennas Propag., vol. 63, no. 4, pp. 1375-1383, April 2015.
[13] P. Mousavi , M. Fakharzadeh, S.H. Jamali, K. Narimani, M. Hossu, Bolandhemmat H., G. Rafi, and S. Safavi- Naeini S “A low-cost ultra low profile phased array system for mobile satellite reception using Zero-Knowledge beamforming algorithm,” IEEE Trans. Antennas Propag., 56, No. 12, 3667–3679, 2008.
[14] N. T. Nguyen, R. Sauleau, M. Ettorre and L. Le Coq, “Focal Array Fed Dielectric Lenses: An Attractive Solution for Beam Reconfiguration at Millimeter Waves,” IEEE Trans. Antennas Propag., vol. 59, no. 6, pp. 2152-2159, June 2011.
[15] A. D. Greenwood and J. Jian-Ming, “A field picture PF wave propagation in inhomogeneous dielectric lenses,” IEEE Antennas Propag. Mag., vol. 41, no. 5, pp. 9-18, Oct. 1999.
[16] J. Thornton, D. Smith, S. J. Foti and Y. Y. Jiang, “Reduced height Luneburg lens antennas for satellite communications-on-the-move,” 2015 Conference on Microwave Techniques (COMITE), 2015, pp. 1-4.
[17] J. Pendry, D. Schurig, and D. Smith, “Controlling electromagnetic fields,” *Science*, vol. 312, no. 5781, pp. 1780-1782, Jun. 2006.
[18] Y. Su and Z. N. Chen, “A Flat Dual-Polarized Transformation-Optics Beamscanning Luneburg Lens Antenna Using PCB-Stacked Gradient Index Metamaterials,” IEEE Trans. Antennas Propag , vol. 66, no. 10, pp. 5088-5097, Oct. 2018.
[19] C. Mateo-Segura, A. Dyke, H. Dyke, S. Haq and Y. Hao, “Flat Luneburg Lens via Transformation Optics for Directive Antenna Applications,” IEEE Trans. Antennas Propag., vol. 62, no. 4, pp. 1945-1953, Apr. 2014.

[20] Y.J. Park, A. Herschlein, and W. Wiesbeck, "A photonic bandgap (PBG) structure for guiding and suppressing surface waves in millimeter-wave antennas," IEEE Trans Microwave Theory Tech., vol. 49, no. 10, pp. 1854-1859, Oct. 2001.
[21] L. Xue and V. F. Fusco, "Printed holey plate Luneburg lens," Microw. Opt. Technol. Lett., vol. 50, pp. 378-380, Dec. 2007.
[22] C. Pfeiffer and A. Grbic, "A Printed, Broadband Luneburg Lens Antenna," IEEE Trans. Antennas Propag., vol. 58, no. 9, pp. 3055-3059, Sep. 2010.
[23] M. Huang, S. Yang, F. Gao, R. Quarfoth and D. Sievenpiper, "A 2-D Multibeam Half Maxwell Fish-Eye Lens Antenna Using High Impedance Surfaces," IEEE Antennas Wireless Propag. Lett., vol. 13, pp. 365-368, 2014.
[24] O. Quevedo-Teruel, J. Miao, M. Mattsson, A. Algaba-Brazalez, M. Johansson, and L. Manholm, "Glide-symmetric fully metallic Luneburg lens for 5G communications at Ka-band," IEEE Antennas Wireless Propag. Lett., vol. 17, no. 9, pp. 1588-1592, 2018.
[25] H. Lu, Z. Liu, Y. Liu, H. Ni and X. Lv, "Compact Air-Filled Luneburg Lens Antennas Based on Almost-Parallel Plate Waveguide Loaded With Equal-Sized Metallic Posts," IEEE Trans. Antennas Propag., vol. 67, no. 11, pp. 6829-6838, Nov. 2019.
[26] Q. Liao, N. J. G. Fonseca, and O. Quevedo-Teruel, "Compact Multibeam Fully Metallic Geodesic Luneburg Lens Antenna Based on Non-Euclidean Transformation Optics," IEEE Trans. Antennas Propag., vol. 66, no. 12, pp. 7383-7388, Dec. 2018.
[27] https://www.thinkom.com/wp-content/uploads/2018/09/ku3030-datasheet_9_18_web.pdf
[28] https://www.thinkom.com/wp-content/uploads/2022/03/thinair-ka2517-datasheet.pdf
[29] N. Gagnon and A. Petosa, "Using rotatable planar phase shifting surfaces to steer a high-gain beam", IEEE Trans. Antennas Propag., vol. 61, no. 6, pp. 3086-3092, Jun. 2013.
[30] M. U. Afzal and K. P. Esselle, "Steering the Beam of Medium-to-High Gain Antennas Using Near-Field Phase Transformation," IEEE Trans. Antennas Propag., vol. 65, pp. 1680-1690, Apr. 2017.
[31] M. Akbari, M. Farahani, A. Ghayekhloo, S. Zarbakhsh, A. Sebak and T. A. Denidni, "Beam Tilting Approaches Based on Phase Gradient Surface for mmWave Antennas," IEEE Trans. Antennas Propag., vol. 68, no. 6, pp. 4372-4385, June 2020
[32] H. Qiu, X. -X. Yang, Y. Yu, T. Lou, Z. Yin and S. Gao, "Compact Beam-Scanning Flat Array Based on Substrate-Integrated Waveguide," in IEEE Transactions on Antennas and Propagation, vol. 68, no. 2, pp. 882-890, Feb. 2020.
[33] Q. Zeng, Z. Xue, W. Ren and W. Li, "Dual-Band Beam-Scanning Antenna Using Rotatable Planar Phase Gradient Transmitarrays," IEEE Trans. Antennas Propag., vol. 68, no. 6, pp. 5021-5026, June 2020
[34] Y. Sun, F. Dang, C. Yuan, J. He, Q. Zhang and X. Zhao, "A Beam-Steerable Lens Antenna for Ku-Band High-Power Microwave Applications," IEEE Trans. Antennas Propag., vol. 68, no. 11, pp. 7580-7583, Nov. 2020.
[35] E. B. Lima, et al., "Circular Polarization Wide-Angle Beam Steering at Ka-Band by In-Plane Translation of a Plate Lens Antenna," IEEE Trans. Antennas Propag., vol. 63, no. 12, pp. 5443-5455, Dec. 2015, doi: 10.1109/TAP.2015.2484419.
[36] S. A. Matos et al., "High Gain Dual-Band Beam-Steering Transmit Array for Satcom Terminals at Ka-Band," IEEE Trans. Antennas Propag., vol. 65, no. 7, pp. 3528-3539, July 2017, doi: 10.1109/TAP.2017.2702658.
[37] L. Di Palma, A. Clemente, L. Dussopt, R. Sauleau, P. Potier, and P. Pouliguen, "Circularly-polarized reconfigurable transmitarray in Ka-band with beam scanning and polarization switching capabilities," IEEE Trans.Antennas Propag., vol. 65, no. 2, pp. 529-540, Feb. 2017.
[38] T. Chaloun, M. Kaynak, W. Menzel, Q. Luo, T. Purtova, S. Gao, V. Ziegler, H. Schumacher, F. Tabarani, and R. Starec, ''Wide-angle scanning active transmit/receive reflectarray,'' IET Microw., Antennas Propag., vol. 8, no. 11, pp. 811-818, Aug. 2014.
[39] P. Naseri, S. A. Matos, J. R. Costa, and C. A. Fernandes, "Phase-delay versus phase-rotation cells for circular polarization transmit arrays – application to satellite Ka-band beam steering," IEEE Trans. Antennas Propag., vol. 66, no. 3, pp. 1236-1247, Mar. 2018.
[40] L. Di Palma, A. Clemente, L. Dussopt, R. Sauleau, P. Potier, and P. Pouliguen, "Circularly-polarized reconfigurable transmitarray in Ka-band with beam scanning and polarization switching capabilities," IEEE Trans. Antennas Propag., vol. 65, no. 2, pp. 529-540, Feb. 2017.
[41] A. Clemente, L. Di Palma, F. Diaby, L. Dussopt, K. Pham, and R. Sauleau, "Electronically-steerable transmitarray antennas for Ka-band," in Proc. 13th Eur. Conf. Antennas Propag., Krakov, Poland, 2019.
[42] R. Stevenson, M. Sazegar, A. Bily, M. Johnson and N. Kundtz, "Metamaterial surface antenna technology: Commercialization through diffractive metamaterials and liquid crystal display manufacturing," 10th Int. Congress on Advanced Electromagnetic Materials in Microwaves and Optics, 2016, pp. 349-351.
[43] G. Minatti, E. Martini, F. Caminita, S. C. Pavone, M. Albani, G. Toso, and S. Maci, "Electronically reconfigurable metasurface antennas based on liquid crystal technology," in Proc. 13th Eur. Conf. Antennas Propag., Krakov, Poland, 2019.
[44] G. M. Rebeiz and L. M. Paulsen, "Advances in SATCOM phased arrays using silicon technologies," IEEE/MTT-S Int. Microwave Symp., Honolulu, HI, USA, 4-9 Jun. 2017, pp. 1877-1879.
[45] J.-C. S. Chieh, E. Yeo, M. Kerber and R. Olsen, "Ku-band dual polarized phased array utilizing silicon beamforming chipsets," IEEE Topical Workshop on Internet of Space, Orlando, FL, USA, 20-23 May 2019, pp. 1-3.
[46] J.-C. S. Chieh, E. Yeo, R. Farkouh, A. Castro, M. Kerber, R. B. Olsen, E. J. Merulla, and S. K. Sharma, "Development of flat panel active phased array antennas using 5G silicon RFICs at Ku- and Ka-bands," IEEE Access, vol. 8, pp. 192669-192681, 2020.
[47] A. H. Aljuhani, T. Kanar, S. Zihir and G. M. Rebeiz, "A scalable dual-polarized 256-element Ku-band SATCOM phased-array transmitter with 36.5 dBW EIRP per polarization," Proc. 48th Eur. Microw. Conf., Madrid, Spain, 23-27 Sep. 2018, pp. 938-941.
[48] G. Gültepe, T. Kanar, S. Zihir, and G. M. Rebeiz, "A 1024-element Ku-band SATCOM phased-array transmitter with 45-dBW single-polarization EIRP," IEEE Trans. Microw. Theory Tech., vol. 69, no. 9, pp. 4157-4168, Sep. 2021.
[49] T. Lambard, O. Lafond, M. Himdi, H. Jeuland, S. Bolioli, and L. Le Coq, "Ka-band phased array antenna for high-data-rate SATCOM," IEEE Antennas Wireless Propag. Lett., vol. 11, pp. 256-259, 2012.
[50] X. Luo, J. Ouyang, Z.-H. Chen, Y. Yan, L. Han, Z. Wu, T. Yu, and K. Zheng, "A scalable Ka-band 1024-element transmit dual-circularly-polarized planar phased array for SATCOM application," IEEE Access, vol. 8, pp. 156084-156095, Aug. 2020.
[51] W. M. Abdel-Wahab H. Al-Saedi, E. Haj Mirza Alian, M. Raeis-Zadeh, A. Ehsandar, A. Palizban, N. Ghafarian, G. Chen, H. Gharaee, M. R. Nezhad-Ahmadi, and S. Safavi-Naeini, "A modular architecture for wide scan angle phased array antenna for K/Ka mobile SATCOM," IEEE MTT-S Int. Microwave Symp., Boston, MA, USA, 2-7 Jun. 2019, pp. 1076-1079.
[52] X. Gu, D. Liu, C. Baks, O. Tageman, B. Sadhu, J. Hallin, L. Rexberg, P. Parida, Y. Kwark, and A. Valdes-Garcia, "Development, implementation, and characterization of a 64-element dual-polarized phased-array antenna module for 28-GHz high-speed data communications," IEEE Trans. Microw. Theory Techn., vol. 67, no. 7, pp. 2975-2984, Jul. 2019.
[53] H. Al-Saedi, W. M. Abdel-Wahab, S. M. Raeis-Zadeh, E. Haj Mirza Alian, A. Palizban, A. Ehsandar, N. Ghafarian, G. Chen, S. Rasti Boroujeni, M.-R. Nezhad-Ahmadi, and S. Safavi-Naeini, "An integrated circularly polarized transmitter active phased-array antenna for emerging Ka-band satellite mobile terminals," IEEE Trans. Antennas Propag., vol. 67, no. 8, pp. 5344-5352, Aug. 2019.
[54] I. Kaplan, I. Marinov, A. Gal, V. Peshlov, M. Gachev, V. Boyanov, and B. Marinov, "Electronically beam steerable antennas for broadband satellite communications," Proc. 8th Eur. Conf. Antennas Propag., The Hague, Netherlands, 6-11 Apr. 2014, pp. 2450-2454.
[55] A. H. Aljuhani, T. Kanar, S. Zihir and G. M. Rebeiz, "A 256-element Ku-band polarization agile SATCOM receive phased array with wide-angle scanning and high polarization purity," IEEE Trans. Microw. Theory Tech., vol. 69, no. 5, pp. 2609-2628, May 2021.
[56] L. Baggen, S. Vaccaro, D. Llorens del Río, J. Padilla and R. T. Sánchez, "A compact phased array for satcom applications," IEEE Int. Symp. Phased Array Systems and Techn., 2013, pp. 232-239.
[57] L. A. Greda and A. Dreher, "Tx-terminal phased array for satellite communication at Ka-band," Eur. Microw. Conf., 2007, pp. 266-269.
[58] G. Gültepe, T. Kanar, S. Zihir, and G. M. Rebeiz, "A 1024-element Ku-band SATCOM dual-polarized receiver with >10-dB/K G/T and embedded transmit rejection filter," IEEE Trans. Microw. Theory Tech., vol. 69, no. 7, pp. 3484-3495, Jul. 2021.
[59] A. Catalani, F. Di Paolo, M. Migliorelli, L. Russo, G. Toso, and P. Angeletti, "Ku-band hemispherical fully electronic antenna for aircraft in

flight entertainment", Hindawi Int. J. Antennas Propag., vol. 2009, no. 230650, pp. 1-7, 2009.
[60] H. Steyskal, A. Hessel, and J. Shmoys, "On the gain-versus-scan tradeoffs and the phase gradient synthesis for a cylindrical dome antenna," IEEE Trans. Antennas Propag., vol. TAP-27, no. 6, pp. 825-831, Nov. 1979.
[61] H. Kawahara, H. Deguchi, M. Tsuji, and H. Shigesawa, "Design of rotational dielectric dome with linear array feed for wide-angle multibeam antenna applications," Electron. Commun. Jpn., Electron., vol. 90, no. 5, pp. 49-57, 2007.
[62] J. Stangel and P. Valentino, "Phased array fed lens antenna," Patent, US3755815A, 1971.
[63] A. Benini, E. Martini, S. Monni, M. Viganò, F. Silvestri, E. Gandini, G. Gerini, G. Toso, and S. Maci, "Phase-gradient meta-dome for increasing grating-lobe-free scan-range in phased arrays", IEEE Trans. Antennas Propag., vol. 66, no. 5, pp. 3973-3982, May 2018.
[64] R. J. Bolt, D. Cavallo, G. Gerini, D. Deurloo, R. Grooters, A. Neto, and G.Toso, "Characterization of a dual- polarized connected-dipole array for Ku-band mobile terminals," IEEE Trans. Antennas Propag., vol. 64, no. 2, pp. 391-398, Feb. 2016.
[65] A. I. Sandhu, E. Arnieri, G. Amendola, L. Boccia, E. Meniconi, and V. Ziegler, "Radiating elements for shared aperture Tx/Rx phased arrays at K/Ka band," IEEE Trans. Antennas Propag., vol. 64, no. 6, pp. 2270–2282, Jun. 2016.
[66] A. J. van Katwijk, A. Neto, G. Toso, and D. Cavallo, "Design of wideband wide-scanning dual-polarized phased array covering simultaneously both the Ku- and the Ka-Satcom bands," 14th Eur. Conf. Antennas Propag., 2020, pp. 1-3.
[67] Y. J. Guo, M. Ansari and N. J. G. Fonseca, "Circuit Type Multiple Beamforming Networks for Antenna Arrays in 5G and 6G Terrestrial and Non-Terrestrial Networks," IEEE J. Microwaves, vol. 1, no. 3, pp. 704-722, July 2021.
[68] Y. Aslan, et al., "Orthogonal Versus Zero-Forced Beamforming in Multibeam Antenna Systems: Review and Challenges for Future Wireless Networks," IEEE J. Microwaves, vol. 1, no. 4, pp. 879-901, Oct. 2021.
[69] J. Butler and R. Lowe, "Beam-forming matrix simplifies design of electronically scanned antennas," Electron. Des., vol. 9, pp. 170-173, Apr. 1961.
[70] A. A. M. Ali, et al., "Design and implementation of two-layer compact wideband Butler matrices in SIW technology for Ku-band applications," IEEE Trans. Antennas Propag., vol. 59, no. 2, pp. 503–512, Feb. 2010.
[71] T. Djerafi and K. Wu, "Multilayered substrate integrated waveguide 4×4 Butler matrix," Int. J. RF Microw. C. E., vol. 22, no. 3, pp. 336-344, May 2012.
[72] T. Tomura, et al., "A 20-GHz-band 64 × 64 hollow waveguide two-dimensional Butler matrix," IEEE Access, vol. 7, pp. 164 080–164 088, Nov. 2019.
[73] J. Nolen, "Synthesis of multiple beam networks for arbitrary illuminations." Ph.D. dissertation, Bendix Corp., Baltimore, MD, Apr. 1965.
[74] N. J. G. Fonseca, "Printed S-band 4×4 Nolen matrix for multiple beam antenna applications," IEEE Trans. Antennas Propag., vol. 57, pp. 1673–1678, June 2009.
[75] T. Djerafi, N. J. G. Fonseca, and K. Wu, "Broadband substrate integrated waveguide 4×4 Nolen matrix based on coupler delay compensation," IEEE Trans. Microw. Theory Tech., vol. 59, pp. 1740–1745, July 2011.
[76] H. Ren, H. Zhang, Y. Jin, Y. Gu, and B. Arigong, "A novel 2-D 3×3 Nolen matrix for 2-D beamforming applications," IEEE Trans. Microw.Theory Tech., vol. 67, pp. 4622–4631, Nov. 2019.
[77] J. Hirokawa and N. J. G. Fonseca, "Generalized One-Dimensional Parallel Switching Matrices With an Arbitrary Number of Beams," IEEE J. Microwaves, vol. 1, no. 4, pp. 975-988, Oct. 2021.
[78] K. Wu, M. Bozzi and N. J. G. Fonseca, "Substrate Integrated Transmission Lines: Review and Applications," IEEE J. Microwaves, vol. 1, no. 1, pp. 345-363, Jan. 2021
[79] C. C. Chang, R. H. Lee, and T. Y. Shih, "Design of a beam switching/steering Butler matrix for phased array system," IEEE Trans. Antennas Propag., vol. 58, no. 2, pp. 367–374, Feb. 2010.
[80] H. N. Chu and T. Ma, ''An extended 4×4 Butler matrix with enhanced beam controllability and widened spatial coverage,'' IEEE Trans. Microw. Theory Techn., vol. 66, no. 3, pp. 1301–1311, Mar. 2018.
[81] K. Ding and A. A. Kishk, ''Extension of Butler matrix number of beams based on reconfigurable couplers,'' IEEE Trans. Antennas Propag., vol. 67, no. 6, pp. 3789–3796, Jun. 2019.
[82] Wallington J.R., "Analysis, Design and Performance of a Microstrip Butler Matrix," 3rd Eur. Microw. Conf., Vol. 1., Oct. 1973.
[83] Q. Yang et al., "A Low Complexity 16×16 Butler Matrix Design Using Eight-Port Hybrids," IEEE Access, vol. 7, pp. 177864-177873, 2019
[84] X. Wang, et al., "28 GHz Multi-Beam Antenna Array based on Wideband High-dimension 16x16 Butler Matrix," 13th Eur. Conf. Antennas Propag. (EuCAP), 2019, pp. 1-4.
[85] S. Kutty and D. Sen, "Beamforming for Millimeter Wave Communications: An Inclusive Survey," IEEE Commun. Surv. Tutor., vol. 18, no. 2, pp. 949-973, 2016
[86] J. Zhang, X. Yu and K. B. Letaief, "Hybrid Beamforming for 5G and Beyond Millimeter-Wave Systems: A Holistic View," IEEE Open J. Commun. Soc., vol. 1, pp. 77-91, 2020
[87] ADAR3000 beamformer IC product page, https://www.analog.com/en/products/adar3000.html
[88] W. Theunissen, V. Jain and G. Menon, "Development of a Receive Phased Array Antenna for High Altitude Platform Stations using Integrated Beamformer Modules," 2018 IEEE/MTT-S International Microwave Symposium - IMS, 2018, pp. 779-782.
[89] Divaydeep Sikri and Rajanik Mark Jayasuriya, "Multi-Beam Phased Array with Full Digital Beamforming for SATCOM and 5G," Microwave Journal, 2019.
[90] Z. Chbili and A. Kerber, "Self-heating impact on TDDB in bulk FinFET devices: Uniform vs Non-uniform Stress", 2016 IEEE International Integrated Reliability Workshop (IIRW), pp. 45-48, 2016.
[91] C. Zhang, F. Zhang, S. Syed, M. Otto and A. Bellaouar, "A Low Noise Figure 28GHz LNA in 22nm FDSOI Technology," 2019 IEEE Radio Frequency Integrated Circuits Symposium (RFIC), 2019, pp. 207-210, doi: 10.1109/RFIC.2019.8701831.
[92] 16 Channel Beamforming Transceiver RFIC Covers the Full 57 to 71 GHz Unlicensed Band, https://www.microwavejournal.com/articles/35968-channel-beamforming-transceiver-rfic-covers-the-full-57-to-71-ghz-unlicensed-band
[93] TRXBF01 product brief https://www.sivers-semiconductors.com/wp-content/uploads/2021/10/Product-Brief-TRXBF01_202110.pdf?hsCtaTracking=ffd4d4e8-646f-4e9b-bc49-e926707743b8%7C27c0226b-c72e-4e06-a05a-065a2e70370f.
[94] A. S. Y. Poon und M. Taghivand, "Supporting and Enabling Circuits for Antenna Arrays in Wireless Communications," Proceedings of the IEEE, Bd. 100, p. 2207–2218, July 2012.
[95] C. Fulton, M. Yeary, D. Thompson, J. Lake und A. Mitchell, "Digital Phased Arrays: Challenges and Opportunities," Proceedings of the IEEE, Bd. 104, p. 487–503, March 2016.
[96] R. Rotman, M. Tur und L. Yaron, "True Time Delay in Phased Arrays," Proceedings of the IEEE, Bd. 104, p. 504–518, March 2016.
[97] D. R. Martinez, R. A. Bond and M. M. Vai, High Performance Embedded Computing Handbook: A Systems Perspective, CRC Press, 2018.
[98] K. Kuhlmann, K. Rezer und A. F. Jacob, "Far field measurement on Ka-band substrate-integrated waveguide antenna array with polarization multiplexing," in 2008 IEEE MTT-S International Microwave Symposium Digest, 2008.
[99] A. Stark, A. Dreher, H. Fischer, A. Geise, R. Gieron, M. Heckler, S. Holzwarth, C. Hunscher, A. F. Jacob, K. Kuhlmann, O. Litschke, D. Lohmann, W. Simon, F. Wötzel und D. Zahn, "SANTANA: Advanced Electronically Steerable Antennas at Ka-Band," in 3rd European Conference on Antennas and Propagation, 2009.
[100] SatixFy, "PRIME- Digital Beam Former ASIC 20," January 2022. [Online]. Available: https://www.satixfy.com/prime/. [Accessed 20 January 2022].
[101] Teledyne e2V, EV12DD700 - Dual channel Ka-band capable 12 GSps DAC, 2022.
[102] SatixFy, "Prime 2.0 - Digital Beamformer ASIC for Flexible Satellite Payloads," 2021.
[103] E. A. Alwan, S. B. Venkatakrishnan, A. A. Akhiyat, W. Khalil und J. L. Volakis, "Code Optimization for a Code-Modulated RF Front End," IEEE Access, Bd. 3, p. 260–273, 2015.
[104] T. Zimmer et al., "SiGe HBTs and BiCMOS Technology for Present and Future Millimeter-Wave Systems," IEEE J. Microwaves, vol. 1, no. 1, pp. 288–298, 2021.
[105] D. Pepe and D. Zito, "Two mm-Wave Vector Modulator Active Phase Shifters With Novel IQ Generator in 28 nm FDSOI CMOS," IEEE J. Solid-State Circuits, vol. 52, no. 2, pp. 344–356, 2017.
[106] K. Takagi, C. Y. Ng, H. Sakurai and K. Matstushita, "GaN MMIC for Ka-Band with 18W," *2015 IEEE Compound Semiconductor Integrated*

Circuit Symposium (CSICS), 2015, pp. 1-4, doi: 10.1109/CSICS.2015.7314504.

[107] C. Y. Ng *et al*., "A 20-Watt Ka-band GaN high power amplifier MMIC," *2014 9th European Microwave Integrated Circuit Conference*, 2014, pp. 404-407, doi: 10.1109/EuMIC.2014.6997878.

[108] B. Schmukler *et al*., "A High Efficiency, Ka-Band, GaN-on-SiC MMIC with Low Compression," *2019 IEEE BiCMOS and Compound semiconductor Integrated Circuits and Technology Symposium (BCICTS)*, 2019, pp. 1-4, doi: 10.1109/BCICTS45179.2019.8972749.

[109] N. Estella, E. Camargo, J. Schellenberg and L. Bui, "High-Efficiency, Ka-band GaN Power Amplifiers," *2019 IEEE MTT-S International Microwave Symposium (IMS)*, 2019, pp. 568-571, doi: 10.1109/MWSYM.2019.8701005.

[110] P. Colantonio and R. Giofré, "A GaN-on-Si MMIC Power Amplifier with 10W Output Power and 35% Efficiency for Ka-Band Satellite Downlink," *2020 15th European Microwave Integrated Circuits Conference (EuMIC)*, 2021, pp. 29-32, doi: 10.1109/EuMIC48047.2021.00019.

[111] https://www.qorvo.com/

[112] https://www.ommic.com/

[113] F. Y. Colomb and A. Platzker, "2 and 4 watt Ka-band GaAs PHEMT power amplifier MMICs," *IEEE MTT-S International Microwave Symposium Digest, 2003*, 2003, pp. 843-846 vol.2, doi: 10.1109/MWSYM.2003.1212501.

[114] I. Ju, H. Ji and I. Yom, "Ku-band GaAs MMIC high power amplifier with high efficiency and broadband," *2015 Conference on Microwave Techniques (COMITE)*, 2015, pp. 1-4, doi: 10.1109/COMITE.2015.7120324.

[115] Keun-Kwan Ryu, Ki-Burm Ahn, Sung-Chan Kim.(2015).A 4W GaAs Power Amplifier MMIC for Ku-band Satellite Communication Applications.JOURNAL OF SEMICONDUCTOR TECHNOLOGY AND SCIENCE,15(4),501-505.

[116] M. Guidry et al., "Demonstration of 30 GHz OIP3/PDC > 10 dB by mm-wave N-polar Deep Recess MISHEMTs," 2019 14th European Microwave Integrated Circuits Conference (EuMIC), 2019, pp. 64-67, doi: 10.23919/EuMIC.2019.8909579.

[117] F. Wang, T.-W. Li, S. Hu, and H. Wang, "A Super-Resolution Mixed-Signal Doherty Power Amplifier for Simultaneous Linearity and Efficiency Enhancement," IEEE J. Solid-State Circuits, vol. 54, no. 12, pp. 3421–3436, 2019.

[118] J. Park, S. Kang, and S. Hong, "Design of a Ka-Band Cascode Power Amplifier Linearized With Cold-FET Interstage Matching Network," IEEE Trans. Microw. Theory Tech., vol. 69, no. 2, pp. 1429–1438, 2021.

[119] F. Wang and H. Wang, "24.6 An Instantaneously Broadband Ultra-Compact Highly Linear PA with Compensated Distributed-Balun Output Network Achieving gt;17.8dBm P<inf>1dB</inf> and gt;36.6% PAE P1dB over 24 to 40GHz and Continuously Supporting 64-/256-QAM 5G NR Signals ," in 2020 IEEE International Solid- State Circuits Conference - (ISSCC), 2020, pp. 372–374.

[120] B. Park et al., "Highly Linear mm-Wave CMOS Power Amplifier," IEEE Trans. Microw. Theory Tech., vol. 64, no. 12, pp. 4535–4544, 2016.

[121] P. Indirayanti and P. Reynaert, "A 32 GHz 20 dBm-PSAT transformer-based Doherty power amplifier for multi-Gb/s 5G applications in 28 nm bulk CMOS," 2017 IEEE Radio Frequency Integrated Circuits Symposium (RFIC), 2017, pp. 45-48, doi: 10.1109/RFIC.2017.7969013.

[122] S. N. Ali, P. Agarwal, J. Baylon, S. Gopal, L. Renaud and D. Heo, "A 28GHz 41%-PAE linear CMOS power amplifier using a transformer-based AM-PM distortion-correction technique for 5G phased arrays," 2018 IEEE International Solid - State Circuits Conference - (ISSCC), 2018, pp. 406-408, doi: 10.1109/ISSCC.2018.8310356.

[123] M. Vigilante and P. Reynaert, "A Wideband Class-AB Power Amplifier With 29–57-GHz AM–PM Compensation in 0.9-V 28-nm Bulk CMOS," in IEEE Journal of Solid-State Circuits, vol. 53, no. 5, pp. 1288-1301, May 2018, doi: 10.1109/JSSC.2017.2778275.

[124] S. Shakib, M. Elkholy, J. Dunworth, V. Aparin and K. Entesari, "2.7 A wideband 28GHz power amplifier supporting 8×100MHz carrier aggregation for 5G in 40nm CMOS," 2017 IEEE International Solid-State Circuits Conference (ISSCC), 2017, pp. 44-45, doi: 10.1109/ISSCC.2017.7870252.

[125] S. M. A. Ali and S. M. R. Hasan, "A 38-GHz Millimeter-Wave Double-Stacked HBT Class-F−1 High-Gain Power Amplifier in 130-nm SiGe-BiCMOS," IEEE Trans. Microw. Theory Tech., vol. 68, no. 7, pp. 3039–3044, 2020.

[126] T.-W. Li, M.-Y. Huang, and H. Wang, "Millimeter-Wave Continuous-Mode Power Amplifier for 5G MIMO Applications," IEEE Trans. Microw. Theory Tech., vol. 67, no. 7, pp. 3088–3098, 2019.

[127] B. Rabet and J. Buckwalter, "A high-efficiency 28GHz outphasing PA with 23dBm output power using a triaxial balun combiner," 2018 IEEE International Solid - State Circuits Conference - (ISSCC), 2018, pp. 174-176, doi: 10.1109/ISSCC.2018.8310240.

[128] C. R. Chappidi, X. Wu and K. Sengupta, "Simultaneously Broadband and Back-Off Efficient mm-Wave PAs: A Multi-Port Network Synthesis Approach," in IEEE Journal of Solid-State Circuits, vol. 53, no. 9, pp. 2543-2559, Sept. 2018, doi: 10.1109/JSSC.2018.2841977.

[129] S. Hu, F. Wang and H. Wang, "2.1 A 28GHz/37GHz/39GHz multiband linear Doherty power amplifier for 5G massive MIMO applications," 2017 IEEE International Solid-State Circuits Conference (ISSCC), 2017, pp. 32-33, doi: 10.1109/ISSCC.2017.7870246.

[130] C. Li, O. El-Aassar, A. Kumar, M. Boenke, and G. M. Rebeiz, "LNA Design with CMOS SOI Process-l.4dB NF K/Ka band LNA," in 2018 IEEE/MTT-S International Microwave Symposium - IMS, 2018, pp. 1484–1486.

[131] Z. Li et al., "A 24–30-GHz TRX Front-End With High Linearity and Load-Variation Insensitivity for mm-Wave 5G in 0.13-μm SiGe BiCMOS," IEEE Trans. Microw. Theory Tech., vol. 69, no. 10, pp. 4561–4575, 2021.

[132] A. A. Nawaz, J. D. Albrecht, and A. Çağrı Ulusoy, "A Ka/V Band-Switchable LNA With 2.8/3.4 dB Noise Figure," IEEE Microw. Wirel. Components Lett., vol. 29, no. 10, pp. 662–664, 2019.

[133] F. Inanlou, C. T. Coen, and J. D. Cressler, "A 1.0 V, 10–22 GHz, 4 mW LNA Utilizing Weakly Saturated SiGe HBTs for Single-Chip, Low-Power, Remote Sensing Applications," IEEE Microw. Wirel. Components Lett., vol. 24, no. 12, pp. 890–892, 2014.

[134] A. Alhamed, O. Kazan, G. Gültepe, and G. M. Rebeiz, "A Multiband/Multistandard 15-57 GHz Receive Phased-Array Module Based on 4 x 1 Beamformer IC and Supporting 5G NR FR2 Operation," IEEE Trans. Microw. Theory Tech., p. 1, 2022.

[135] T. A. Ozkan, A. Burak, I. Kalyonc, M. Kaynak, and Y. Gurbuz, "A High-Gain SiGe BiCMOS LNA for 5G In-Band Full-Duplex Applications," in 2020 15th European Microwave Integrated Circuits Conference (EuMIC), 2021, pp. 53–56.

[136] V. Issakov and A. Werthof, "A 10 mW LNA with Temperature Compensation for 24 GHz Radar Applications in SiGe BiCMOS," in 2020 IEEE BiCMOS and Compound Semiconductor Integrated Circuits and Technology Symposium (BCICTS), 2020, pp. 1–4.

[137] Q. Ma, D. M. W. Leenaerts, and P. G. M. Baltus, "Silicon-Based True-Time-Delay Phased-Array Front-Ends at Ka-Band," IEEE Trans. Microw. Theory Tech., vol. 63, no. 9, pp. 2942–2952, 2015.

[138] A. A. Alhamed and G. M. Rebeiz, "A 28–37 GHz Triple-Stage Transformer-Coupled SiGe LNA with 2.5 dB Minimum NF for Low Power Wideband Phased Array Receivers," in 2020 IEEE BiCMOS and Compound Semiconductor Integrated Circuits and Technology Symposium (BCICTS), 2020, pp. 1–4.

[139] J. Zhang, D. Zhao, and X. You, "Analysis and Design of a CMOS LNA With Transformer-Based Integrated Notch Filter for <italic>Ku</italic>-Band Satellite Communications," IEEE Trans. Microw. Theory Tech., vol. 70, no. 1, pp. 790–800, 2022.

[140] H. Chen, H. Zhu, L. Wu, Q. Xue, and W. Che, "A 7.2–27.3 GHz CMOS LNA With 3.51 ±0.21 dB Noise Figure Using Multistage Noise Matching Technique," IEEE Trans. Microw. Theory Tech., vol. 70, no. 1, pp. 74–84, 2022.

[141] J.-F. Chang and Y.-S. Lin, "A 13.7-mW 21-29-GHz CMOS LNA With 21.6-dB Gain and 2.74-dB NF for 28-GHz 5G Systems," IEEE Microw. Wirel. Components Lett., pp. 1–4, 2021.

[142] Z. Deng, J. Zhou, H. J. Qian, and X. Luo, "A 22.9–38.2-GHz Dual-Path Noise-Canceling LNA With 2.65–4.62-dB NF in 28-nm CMOS," IEEE J. Solid-State Circuits, vol. 56, no. 11, pp. 3348–3359, 2021.

[143] Y. Wang et al., "A Ka-Band SATCOM Transceiver in 65-nm CMOS With High-Linearity TX and Dual-Channel Wide-Dynamic-Range RX for Terrestrial Terminal," IEEE J. Solid-State Circuits, p. 1, 2021.

[144] H.-W. Choi, C.-Y. Kim, and S. Choi, "6.7–15.3 GHz, High-Performance Broadband Low-Noise Amplifier With Large Transistor and Two-Stage Broadband Noise Matching," IEEE Microw. Wirel. Components Lett., vol. 31, no. 8, pp. 949–952, 2021.

[145] H. Chen, H. Zhu, L. Wu, W. Che, and Q. Xue, "A Wideband CMOS LNA Using Transformer-Based Input Matching and Pole-Tuning Technique," IEEE Trans. Microw. Theory Tech., vol. 69, no. 7, pp. 3335–3347, 2021.

[146] S.-M. Hwang and K.-H. Lee, “Comparison of ESD Immunity Between GaAs-Based LNA and SiGe-Based LNA,” IEEE Trans. Electromagn. Compat., vol. 54, no. 4, pp. 944–946, 2012.
[147] L. Pace et al., "DC Power-Optimized Ka-Band GaN-on-Si Low-Noise Amplifier With 1.5 dB Noise Figure," in IEEE Microwave and Wireless Components Letters.